Vibrational Energy Pooling in CO on NaCl(100): Simulation and Isotope Effects†

S. A. Corcelli and J. C. Tully*

Department of Chemistry, Yale University, P.O. Box 208107, New Haven, Connecticut 06520-8107

Received: February 22, 2002; In Final Form: May 31, 2002

The phenomenon of vibrational energy pooling in a CO monolayer on a NaCl(100) surface is investigated using a kinetic simulation approach. The kinetic Monte Carlo (KMC) method requires as input the rate constants for each available channel of vibrational energy flow in the system: laser excitation; vibrational relaxation to the substrate; vibrational energy transfer between nearest neighbor CO molecules on the surface; radiation. These rates were computed using perturbation theory and available experimental information. Our simulations predict a dramatic isotope effect in which energy is seen to preferentially pool on heavier isotopomers of CO if a natural abundance sample of CO is optically pumped. Simulations of an isotopically pure CO/NaCl(100) system continuously pumped by a laser source demonstrate that vibrational energy pools containing more and more quanta can be formed by using more intense lasers until a theoretical crossover is reached where vibrational relaxation rates become faster than vibrational energy pooling rates. This crossover occurs at $n = 18$ for $^{12}C^{16}O$. Finally, the effect of temperature on the vibrational dynamics in the CO/NaCl(100) system is explored with the result that finite temperature facilitates energy redistribution within the monolayer, hastening the overall vibrational relaxation dynamics.

I. Introduction

CO adsorbed onto the (100) face of the NaCl crystal has been referred to as a model for the study of physisorbed molecule/surface systems.[1,2] At temperatures above 35 K, polarized infrared spectroscopic (PIRS)[3−8] measurements along with helium atom scattering (HAS)[9] experiments have revealed the monolayer to have a (1×1) disordered structure containing 1 CO molecule/unit cell. On average, the CO molecules are adsorbed perpendicular to the NaCl(100) surface directly above Na^+ ions with the carbon end of the CO molecule closest to the surface.[10] Below 35 K the monolayer undergoes a phase change to an ordered (2×1) structure which contains 2 distinguishable CO molecules/unit cell each tilted by roughly 25° to the surface normal in opposite directions. Using this experimentally determined structural information, accurate potential energy surfaces have been devised and used to conduct molecular dynamics (MD) simulations to further investigate the nature of the $(2 \times 1) \rightarrow (1 \times 1)$ phase transition.[11,12] These simulations suggest dynamical effects in the (2×1) monolayer are responsible for the order/disorder transition manifested as temperature is increased above 35 K.

The CO/NaCl(100) has also served as a model system for exploring the dynamics of vibrational energy flow at surfaces.[1,2] Extensive time-domain infrared spectroscopic measurements by Ewing and co-workers have revealed some interesting properties of vibrational energy flow within the CO monolayer on the NaCl(100) surface, including the phenomenon of vibrational energy pooling.[13−17] A mechanism for vibrational energy pooling in a gas phase system of diatomic molecules being optically pumped by a laser tuned to their fundamental vibrational absorption frequency was first proposed in 1968 by Treanor et al.[18] When a pair of diatomic molecules each in their first vibrationally excited state collide, a vibrational exchange reaction of the type $AB(1) + AB(1) \rightarrow AB(0) + AB(2)$ can occur. Anharmonicity in the bond vibration of the molecules results in the products being lower in energy than the reactants, the excess energy being transferred to the translations and rotations of the molecules after the collision. Thus, anharmonicity provides a thermodynamic driving force for vibrational energy pooling provided the molecules interact strongly for the vibrational exchange to occur, and there is an available channel to dissipate the excess energy. In a CO monolayer on the NaCl-(100) surface the molecules are close enough to interact with nearest-neighbor separation of 3.96 Å,[19] and the phonons of the NaCl substrate provide a bath to soak up the excess energy from vibrational energy pooling reactions. Furthermore, the tremendous mismatch between the vibrational frequency of the CO molecule (∼2100 cm^{-1}) and the highest phonon frequency (∼223 cm^{-1})[19] make vibrational relaxation to the substrate inefficient and slow providing more opportunity for vibrational energy pooling to occur. Evidence for vibrational energy pooling in the CO/NaCl(100) system was obtained in an experiment by Chang and Ewing.[13] In their experiment, a carefully prepared monolayer of $^{13}C^{16}O$ held at 22 K was pumped with a 25 μJ pulse of 2107.40 cm^{-1} light for 5 μs. Following the excitation pulse the overtone fluorescence emanating from the surface was monitored as a function of time to reveal an exponential decay with a long time constant of 4.3 ms, providing an indication of just how long energy persists in the CO monolayer before relaxation. When spectral filters were used to block overtone fluorescence from reaching the detector, it was determined that most of the fluorescence was in the range 3400−4200 cm^{-1} and must have originated from CO molecules in their $n = 2$ to $n = 15$ vibrationally excited states.

Following our previous work simulating Chang and Ewing's experiment,[20] our strategy is to identify all of the relevant vibrational energy flow pathways in CO/NaCl(100) system, calculate their rate constants, and then use a kinetic Monte Carlo method[21−25] to simulate the overall vibrational dynamics in the monolayer. A similar approach was taken by Lee et al. to

† Part of the special issue "R. Stephen Berry Festschrift".

10.1021/jp0205012 CCC: $22.00
Published on Web 08/16/2002

analyze the results of their experiment in which gaseous mixtures of N_2/CO and N_2/CO/O_2 were optically pumped.[26] The vibrational energy flow pathways in the CO/NaCl(100) system are as follows: (1) Optical absorption occurs, whereby a CO molecule is excited from its vibrational ground state $n = 0$ to its vibrational excited state $n = 1$ by absorption of infrared light, CO(0) $\rightarrow$ CO(1). We make the assumption that $n = 0 \rightarrow 1$ is the only possible absorption process, and its rate constant depends on the laser intensity and incident angle for the experiment being modeled. (2) Vibrational relaxation occurs, whereby a CO molecule relaxes from vibrational state n to $n - 1$ by emitting phonons in the NaCl(100) substrate, CO(n) $\rightarrow$ CO($n - 1$). Multiple quantum transitions in the CO molecule are neglected throughout this work because they are forbidden in the dipole approximation. In section IIA we present the rates of single quantum vibrational relaxation as a function of initial vibrational quantum state n for $^{12}C^{16}O$ and $^{13}C^{16}O$. The details of how these rates were obtained are contained in a separate publication.[20,27] These rates were obtained for a model in which the CO molecule is treated as a Morse oscillator, and the NaCl(100) phonon bath is treated as a collection of harmonic oscillators with a spectral density described by the Debye model coupled to the deformation potential approximation.[28,29] Following the work of Egorov and Skinner[30] on multiphonon vibrational relaxation rates in solids, we obtain a closed-form analytical expression for the vibrational relaxation rate using perturbation theory. (3) Nonresonant single-quantum vibrational energy transfer occurs, where two CO molecules, assumed to be nearest neighbors on the NaCl(100) surface, exchange a single quantum of vibrational energy, CO(n) + CO(m) $\rightarrow$ CO($n - 1$) + CO($m + 1$), and the products are different in energy than the reactants, i.e., $n \neq m + 1$. In section IIA the rates of single quantum nonresonant vibrational energy transfer as a function of initial quantum states n and m are presented. These rates were obtained for a model in which two Morse oscillator CO molecules, assumed to be nearest neighbors and exactly perpendicular to the NaCl(100) surface, interact laterally through a dipole−dipole potential. The underlying NaCl substrate is again treated as a collection of harmonic oscillators with a Debye density of states, and the rates are calculated using perturbation theory. The details of these calculations were presented in a separate publication.[20,27] (4) Resonant single quantum vibrational energy transfer occurs, where again two CO molecules, assumed to be nearest neighbors on the NaCl(100) surface, exchange a single quantum of vibrational energy, where the net effect of the single-quantum energy transfer is CO($n + 1$) + CO(n) $\rightarrow$ CO(n) + CO($n + 1$). Since the reactants and products are isoenergetic in this class of V−V energy transfer, no energy dissipation is necessary for this process to occur. As described in section IIA we estimate the rates of single-quantum resonant V−V energy transfer as a function of initial quantum state n for a model in which two Morse oscillator CO molecules, assumed to be nearest neighbors on the NaCl(100) surface, interact laterally through a dipole−dipole potential. (5) Single quantum fluorescence occurs, by which a CO molecule radiates a photon and relaxes from vibrational state n to state $n - 1$, CO(n) $\rightarrow$ CO($n - 1$). The fluorescence rate for the relaxation of a CO molecule from its first vibrationally excited state $n = 1$ to its ground vibrational state $n = 0$ has been determined from a measurement of the fundamental infrared absorption cross section of CO on NaCl(100) as $k_1 = 10.9\ s^{-1}$.[17] Using standard spectroscopic relationships, along with the experimentally determined value for k_1, the rates for single quantum fluorescence as a function of initial quantum state n can be calculated.

This treatment assumes that vibrational dephasing is fast relative to other rate processes. It has been determined that the position and line width of the infrared absorption of CO on NaCl(100) both display the same exponential dependence on temperature.[16] This observation is consistent with vibrational dephasing being the primary broadening mechanism, and thus the line width gives a reasonable measure of the vibrational dephasing rate.[31,32] Temperature-dependent infrared absorption line width measurements have revealed a vibrational dephasing rate of approximately $10^{11}\ s^{-1}$.[16] Rapid vibrational dephasing acts to localize vibrational energy onto specific CO molecules after coherent excitation of the monolayer from the external laser source. However, vibrational dephasing occurs so quickly that explicit consideration of this effect does not alter the vibrational population dynamics in this system. This justifies the localized excitation hopping model employed here.

Vibrationally induced desorption is ignored in this work. The rate of desorption of CO molecules from the NaCl(100) surface after excitation with a 5 μJ infrared pulse for 5 μs was estimated to be $\leq 10^{-4}\ s^{-1}$ by Chang and Ewing.[17] This process occurs so slowly that it also does not affect the vibrational population dynamics. The slow vibrationally induced desorption rate is also indirect evidence that vibrational energy in CO molecules does not couple efficiently to the frustrated translation and rotations of the CO molecules. This allows us to leave these motions out of our models completely, because they do not contribute as strongly as phonon excitation to any of the vibrational energy dissipation processes relevant in the CO/NaCl(100) system. This has been demonstrated by molecular dynamics simulations[33] and is consistent with the observation that no vibrationally induced desorption is detected in this system.[17]

In the time-dependent fluorescence experiment on the CO/NaCl(100) by Chang and Ewing,[13] an isotopically pure sample of $^{13}C^{16}O$ was used. In other experiments performed on gaseous and solid CO samples containing a natural abundance concentration of the various CO isotopomers, 98.66% $^{12}C^{16}O$, 1.10% $^{13}C^{16}O$, and 0.24% of the other isomers $^{12}C^{17}O$, $^{12}C^{18}O$, $^{13}C^{17}O$, and $^{13}C^{18}O$, vibrational energy was seen to preferentially pool to the heaviest isotopes in the sample.[26,34] Diatomic molecules containing heavier isotopes have slightly lower vibrational energy levels than their lighter counterparts. In particular, for CO,

$$^{12}C^{16}O \xrightarrow{\Delta\omega = -25\ cm^{-1}} {}^{12}C^{17}O \xrightarrow{\Delta\omega = -22\ cm^{-1}} {}^{13}C^{16}O \xrightarrow{\Delta\omega = -4\ cm^{-1}} {}^{12}C^{18}O \xrightarrow{\Delta\omega = -48\ cm^{-1}} {}^{13}C^{18}O \quad (1)$$

Therefore, pooling energy in the heavier isotopes is preferred over pooling in the lighter isotopes. Rate constants have been calculated for vibrational energy transfer between different CO isotopomers in the gas phase.[35,36] Following our previous work simulating the Chang and Ewing experiment,[20] in section IIA we discuss rate constants for vibrational relaxation and vibrational energy transfer for a system containing $^{12}C^{16}O$ and $^{13}C^{16}O$ molecules adsorbed on the NaCl(100) surface. With these rates in hand, we were then able to simulate a pulsed laser experiment for CO/NaCl(100) containing roughly 99% $^{12}C^{16}O$ and 1% $^{13}C^{16}O$ with a kinetic Monte Carlo (KMC) method outlined in section IIB. The results of the simulations are presented in section IIIA and predict a significant isotope effect in the vibrational energy pooling dynamics in the CO/NaCl(100) system.

TABLE 1: Bond Vibration Parameters for $^{12}C^{16}O$ and $^{13}C^{16}O$ on NaCl (100), Assuming a Morse Potential Having the Form $V(x) = D(e^{-2\alpha x} - 2e^{-\alpha x})$[a]

param	$^{12}C^{16}O$	$^{13}C^{16}O$	param	$^{12}C^{16}O$	$^{13}C^{16}O$
α (Å^{-1})	2.21	2.21	ω_{10} (cm^{-1})	2154.8	2107.4
D (eV)	12.2	12.2	ω_{21} (cm^{-1})	2130.7	2084.4
μ (amu)	6.86	7.17			

[a] In the equation x is the displacement of the bond from its equilibrium value, D is the dissociation energy of the molecule, α is an empirical constant, and μ is the reduced mass of the molecule. D and α were chosen such that the transition frequencies $\omega_{10} \equiv E_1 - E_0$ and $\omega_{21} \equiv E_2 - E_1$ precisely agree with their experimentally measured values for $^{13}C^{16}O$ on NaCl(100).

In section IIIB we turn our attention to simulating an experiment that has not been performed on the CO/NaCl(100) system, one in which a continuous-wave (CW) laser vibrationally excites CO molecules from $n = 0$ to $n = 1$. Vibrational energy is continuously pumped into the system, but at the same time energy is being dissipated to the NaCl(100) substrate. After some time has passed, these two processes balance one another and the vibrational state of the system will reach a steady state. The effect of the CW laser intensity on the steady-state vibrational population distributions is explored.

Finally, in section IIIC we return our attention to the time-dependent fluorescence experiment to study the effect of finite temperature on the vibrational dynamics in the CO/NaCl(100) system. Energetically uphill energy hops, CO(n) + CO(0) $\rightarrow$ CO($n - 1$) + CO(1), not possible at zero temperature, are identified as providing a mechanism by which vibrational energy may be redistributed within the monolayer. This redistribution of vibrational quanta within the monolayer leads to accelerated dissipation of energy from the CO monolayer into the underlying NaCl substrate. Concluding remarks are made in section IV.

II. Methods

A. Rate Constants. There are two primary pathways of vibrational energy flow in the CO on NaCl(100) system, vibrational relaxation, CO(n) $\rightarrow$ CO($n - 1$), and vibrational energy hopping between nearest neighbor CO molecules, CO(n) + CO(m) $\rightarrow$ CO($n + 1$) + CO($m - 1$). To simulate the vibrational energy flow within the entire CO monolayer we must have at hand the rate constants for both of these processes as a function of the vibrational quantum numbers n and m.

In the rate constant calculations we begin by assuming a model whose Hamiltonian can be separated into the convenient form

$$H = H_S + H_B + V \tag{2}$$

When the vibrational relaxation of a single CO molecule on the NaCl(100) surface is considered, the system part of the Hamiltonian, H_S, is taken to be that of a Morse oscillator with parameters as listed in Table 1. The bath part of the Hamiltonian, H_B, represents the underlying NaCl substrate modeled as a collection of harmonic oscillators with the conventional choice of spectral density, $\Gamma(\omega)$, for problems involving energy relaxation by acoustic phonons, namely the Debye model coupled with the deformation potential approximation,[29,37]

$$\Gamma(\omega) = \begin{cases} \lambda \dfrac{4\omega^3}{{\omega_D}^4} & 0 \le \omega \le \omega_D \\ 0 & \omega > \omega_D \end{cases} \tag{3}$$

where ω_D is the Debye frequency of the NaCl substrate, 223 cm^{-1},[19] and $\Gamma(\omega)$ is normalized to the dimensionless empirical parameter $\lambda = 0.552$, which governs the overall strength of the system−bath coupling. λ is the single free parameter in the model and was self-consistently chosen such that decay constant for the fluorescence intensity decay curve simulated using KMC methods agrees with the experimental value measured by Chang and Ewing for $^{13}C^{16}O$ on NaCl(100) at 22 K after irradiation with a 25 μJ pulse of 2107.4 cm^{-1} infrared laser light for 5 μs. The choice of the parameter λ is discussed at greater length in a previous publication.[20] Finally, the form of the potential energy which binds the CO molecule to the NaCl(100) surface and is ultimately responsible for the relaxation of energy from the CO bond vibration and the NaCl bath[38−40] is assumed to be of the Morse form

$$V = D'\left\{\exp\left[-2\alpha'\left(\frac{m_O}{M_{CO}}x - z\right)\right] - 2\exp\left[-\alpha'\left(\frac{m_O}{M_{CO}}x - z\right)\right]\right\} \tag{4}$$

where z is the displacement perpendicular to the substrate surface of the Na^+ ion directly beneath the CO molecule, D' is the energy required to desorb the CO molecule (0.168 eV), and α' is an empirical constant of the Morse potential (0.82 Å^{-1}); primes are used to distinguish from the CO bond vibration Morse potential energy parameters. m_O is the mass of the oxygen atom, and M_{CO} is the mass of the entire CO molecule. The quantity $(m_O/M_{CO})x - z$ represents the distance between the carbon atom of the CO molecule and the Na^+ ion, assuming the center of mass of the CO molecule remains stationary. α' was chosen such that the first vibrational transition frequency of the entire CO molecule oscillating perpendicular to the NaCl(100) surface matches the value 69 cm^{-1} determined from molecular dynamics simulations,[12] assuming a reduced mass appropriate for $^{13}C^{16}ONa^+$ (12.8 amu). The rate constants for single quantum vibrational relaxation were obtained by closely following the work of Egorov and Skinner[30] and specializing their perturbation theory results to our model Hamiltonian. The details of how these rate constants are calculated are the subject of a separate publication.[20,27]

The filled circles and squares in Figure 1 are the vibrational relaxation rate constants, W_n, for $^{12}C^{16}O$ and $^{13}C^{16}O$ shown as a function of n, the initial vibrational state of the CO molecule. The approximations used to arrive at the rate constants for multiphonon vibrational relaxation of a CO molecule on NaCl(100) require (1) that the temperature of the bath be sufficiently low such that few phonons are thermally active in the NaCl crystal and can be involved in phonon absorption processes and (2) that the relaxation process be mediated by more than roughly 3 phonons. Both requirements are well satisfied since the experiments we are interested in simulating were conducted at 22 K ($k_BT = 15.3$ cm^{-1}) and, for all of the relevant vibrational states of CO on NaCl(100) in this study, $1 \le n \le 30$, the minimum number of phonons needed to relax a single quantum of CO vibration is $p = 7$.

There are several features to note regarding the vibrational energy relaxation rates shown in Figure 1. The vibrational relaxation rates for both isotopomers are very nearly exponential and increase as a function of n. This is because, as n increases, ω_n, the energy gap between vibrational states n and $n - 1$, decreases, meaning the energy can be dissipated by a lower order phonon process in the bath. The nearly exponential growth in the relaxation rate as a function of decreasing energy gap agrees with phenomenological exponential energy gap laws seen in a wide variety of relaxation experiments.[30,41−47] The vibra-

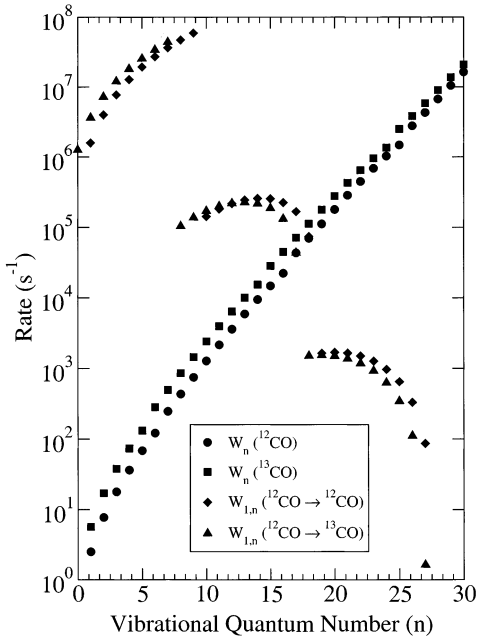

Figure 1. Rate constants W_n for single-quantum vibrational relaxation, CO(n) → CO(n − 1), for $^{12}C^{16}O$ (filled circles) and $^{13}C^{16}O$ (filled squares) on the NaCl(100) surface. Also shown are the rate constants $W_{n,1}$ for single-quantum vibrational exchange between nearest neighbor CO molecules on the NaCl(100) surface, CO(n) + *CO*(1) → *CO*(n + 1) + *CO*(0), for $^{12}C^{16}O$ → $^{12}C^{16}O$ (filled diamonds) and $^{12}C^{16}O$ → $^{13}C^{16}O$ (filled triangles). These results were obtained using the methods described in section IIA with parameters listed in Table 1.

tional relaxation rate of the heavier isotopomer, $^{13}C^{16}O$, is faster for all values of n. $^{13}C^{16}O$, being the heavier isotopomer, vibrates at a slightly lower frequency than $^{12}C^{16}O$. This means the energy gap, ω_n, is slightly smaller for $^{13}C^{16}O$ than $^{12}C^{16}O$ and, thus, vibrational relaxation rates for $^{13}C^{16}O$ should be faster than those for $^{12}C^{16}O$ as is seen in Figure 1. Finally, the fundamental vibrational relaxation rate for $^{13}C^{16}O$ to relax from vibrational state $n = 1$ to its ground vibrational level is determined to be 5.69 s^{-1}. This result is much slower than the mean 233 s^{-1} fluorescence intensity decay rate observed in Chang and Ewing's experiment[13] since the latter is dominated by higher n molecules which relax faster.

We also need to consider the second primary channel of vibrational energy flow in the CO/NaCl(100) system, vibrational energy hopping within the CO monolayer, CO(n) + CO(m) → CO(n − 1) + CO(m + 1). Once again, the starting point is to assume a model whose Hamiltonian can be separated into system, bath, and interaction pieces as shown in eq 2. The bath part of the Hamiltonian describing the underlying NaCl substrate is the same as was described above for the vibrational relaxation model, a collection of harmonic oscillators with frequencies distributed according to a standard Debye density of states. The system part of the Hamiltonian, however, must be modified to include a pair of anharmonic CO molecules. We assume that vibrational energy hopping can only occur between two CO molecules that are nearest neighbors on the CO separated by an average distance $R_0 = 3.96$ Å and that these molecules are aligned exactly parallel to each other and perpendicular to the NaCl(100) surface. The bond vibration coordinate for both CO molecules is described by a Morse oscillator Hamiltonian with parameters listed in Table 1. For the two CO molecules to exchange a vibrational quanta of energy and at the same time dissipate excess energy into the NaCl(100) substrate if the vibrational energy hop is nonresonant, the CO molecules must be coupled to each other and to the bath. The lowest order electrostatic interaction between the two CO molecules is dipole−dipole having the form

$$V = \frac{\mu_1(x_1)\mu_2(x_2)}{R^3} \tag{5}$$

where μ_1 and μ_2 are the electric dipoles moments of CO molecule 1 and 2, which depend on their respective bond vibration coordinates x_1 and x_2, and R is the spatial separation between the molecules. The separation R can be written as a sum of the average equilibrium displacement R_0 and a relative displacement, $y = y_1 + y_2$, resulting from the lateral motion of the Na^+ ions directly beneath each CO molecule. The interaction potential energy depends on the two system coordinates x_1 and x_2, as well as the bath coordinates y_1 and y_2, and will allow for nonresonant vibrational energy hops between the two molecules. Perturbation theory can again be applied to obtain the rate constants for single quantum vibrational energy hopping. The details of how these rate constants are calculated are the subject of a separate publication.[20,27]

The filled diamonds and triangles in Figure 1 are a particular class of single-quantum vibrational energy hopping rate constants, $W_{1,n}$. The energy transfer rate $W_{1,n}$ represents the rate for a CO molecule in it first vibrationally excited state to donate its vibrational quantum to a neighboring CO molecule. This is the principle mechanism for the formation of vibrational energy pools, CO(1) + CO(1) → CO(0) + CO(2), as well as for their subsequent growth, CO(1) + CO(n) → CO(0) + CO(n + 1). In Figure 1 the rates depicted by the filled diamonds are for energy hops between a pair of $^{12}C^{16}O$ molecules and those depicted by the filled triangles are for energy transfer from the lighter isotopomer, $^{12}C^{16}O$, to the heavier isotopomer, $^{13}C^{16}O$. The first thing immediately noticeable about both sets of vibrational energy hopping rates are the discontinuities in the rate constant curve as a function of vibrational quantum number n. These discontinuities result because the energy that needs to be dissipated to the bath, $\omega_{n,1}$, suddenly exceeds the Debye frequency of NaCl substrate and, thus, needs to be dissipated by successively higher order phonon processes. For a more realistic density of states the discontinuities would much less pronounced.

For $n \leq 12$ the rate of vibrational energy transfer from a light CO molecule to a heavy CO molecule exceeds the rate of energy transfer among light CO molecules. This is because, for small values of n, the energy to be dissipated in a nonresonant energy pooling event, $\omega_{1,n}$, can be dissipated by exciting a single phonon in the bath. Since the Debye density of states grows with increasing frequency, the process that requires *more* energy to be dissipated by a single phonon will have a faster rate. Because $^{13}C^{16}O$ vibrates at a lower frequency than $^{12}C^{16}O$, $\omega_{1,n}$ is larger for $^{13}C^{16}O$ than it is for $^{12}C^{16}O$, and thus energy transfer from the lighter isotopomer to the heavy isotopomer will occur with a faster rate as is seen in Figure 1. This also means that energy should preferentially begin pooling at $^{13}C^{16}O$ versus $^{12}C^{16}O$, a conclusion which is confirmed in our KMC simulations discussed below. By contrast, for larger values of n the energy $\omega_{1,n}$ exceeds the Debye frequency of the NaCl substrate and must be dissipated by multiple phonons. In this case, having to dissipate more energy is a hindrance and causes the vibrational energy transfer events among light CO molecules to occur more rapidly than vibrational energy transfer from light to heavy CO molecules.

Note that in Figure 1 the first discontinuity in the $W_{1,n}$ rate constant curve occurs at a smaller value of the vibrational

quantum number n for $^{13}C^{16}O$ than it does for $^{12}C^{16}O$; $n = 7$ for $^{13}C^{16}O$ compared to $n = 9$ for $^{12}C^{16}O$. This first discontinuity in the rate constant curve represents the transition from nonresonant energy hops where the excess energy $\omega_{1,n}$ is dissipated by two phonons as opposed to one. The location of the discontinuity also signifies a dynamical bottleneck in the vibrational energy pooling process. The result of a process with rate $W_{1,n}$ is to produce a CO molecule in vibrational state $n + 1$. If energy is relatively scarce in the system, such as the case in the experiment of Chang and Ewing, few CO molecules will be pumped much beyond this bottleneck. Thus, in a system composed mostly of $^{12}C^{16}O$ with just a few $^{13}C^{16}O$ molecules it is expected that energy pools in $^{12}C^{16}O$ molecules will be a bit more intense than in $^{13}C^{16}O$ molecules. Simulation results presented in section IIIA demonstrate this aspect of the isotope effect in vibrational energy pooling in a mixed-isotope sample.

Rate constants for the nonresonant energy transfer events between CO molecules on the NaCl(100) surface were computed for all combinations of initial vibrational states n and m for which the energy to be dissipated to the bath was positive. However, "backward" vibrational energy hops in which the system must extract an activation energy from the bath are also possible at finite temperatures. The backward rates were computed from the forward rates using the detailed balance relation

$$W_{n,m} = W_{m-1,n+1} e^{\beta \omega_{n,m}} \tag{6}$$

The important role of backward vibrational energy hops will be explored in section IIIB.

A final channel of vibrational energy flow in the CO/NaCl(100) system we have not yet fully discussed in this section is resonant vibrational energy hopping. As energy is introduced into the CO monolayer from an external laser source, a certain fraction of CO molecules is excited to its $n = 1$ vibrational state. These vibrational quanta first localize onto specific CO molecules because of rapid vibrational dephasing occurring on a 10 ps time scale. The next fastest vibrational energy flow process available in the system is the resonant energy transfer processes $CO(1) + CO(0) \rightarrow CO(0) + CO(1)$. The presence of this type of resonant process implies that single quanta of vibrational energy can flow almost freely via rapid resonant energy transfer between singly excited CO molecules and more abundant ground state CO molecules. The mobility of energy in the monolayer contributes greatly to vibrational energy pooling.

Conceptually, resonant energy hopping is simpler than nonresonant hopping since there is no need for the pair of CO molecules to dissipate energy to the bath to undergo an energy transfer. In general, for a single quantum vibrational energy hop to be resonant the initial state of the system must be $|I\rangle = |n + 1,n\rangle$ with a corresponding final state $|F\rangle = |n,n + 1\rangle$, where $n \geq 0$. Taking $|I\rangle$ and $|F\rangle$ as a resonant two-level system with an interaction potential energy given by eq 5, it is easy to show that the probability of remaining in state $|I\rangle$ after some time t has passed oscillates coherently as $\cos^2(V_{FI}t)$, where V_{FI} is the matrix element of the interaction potential energy given by eq 5; $V_{FI} = \langle F|V|I\rangle$. Rapid vibrational dephasing destroys the coherent oscillation of population between $|I\rangle$ and $|F\rangle$ allowing us to define a crude rate for the transition as the inverse of the time it takes for the population in the initial state to decay by 1/e. For the case where $|I\rangle = |1,0\rangle$ the rate is 6.37×10^{10} s^{-1} for a pair of $^{12}C^{16}O$ molecules and 6.23×10^{10} s^{-1} for a pair of $^{13}C^{16}O$ molecules, which is several orders of magnitude larger than the rates of nonresonant vibrational energy transfer and vibrational relaxation shown in Figure 1. The $|1,0\rangle \rightarrow |0,1\rangle$ vibrational energy transfer process is no longer resonant if it is between a $^{12}C^{16}O$ and $^{13}C^{16}O$, because of the slightly different vibrational level structure in the two isotopomers. This is significant because a single quanta of vibrational energy will constitute a stable pool of energy in a $^{13}C^{16}O$ molecule when it is surrounded by $^{12}C^{16}O$ molecules, as opposed to the two quanta of vibrational energy constituting a stable pool in the surrounding $^{12}C^{16}O$ molecules.

Since the resonant rates are much larger than all other energy flow rates in the system, it is found that the KMC simulations of the vibrational dynamics of the CO/NaCl(100) system are almost completely insensitive to the exact value of the resonant transfer rates over several orders of magnitude. Thus, our crude estimate for the resonant energy transfer rates is sufficient to capture the qualitative effect of the resonant energy transfer rates on the overall vibrational dynamics in the CO/NaCl(100) system.

B. Kinetic Monte Carlo Methods. Kinetic Monte Carlo (KMC) methods can be utilized to simulate the detailed vibrational dynamics within the CO monolayer on NaCl(100) by numerically solving the Master equation for the time evolution of the vibrational population distribution $P_n(t)$.[21−25] $P_n(t)$ is the average probability of finding a CO molecule in vibrational state n at time t. The Master equation for the time evolution of $P_n(t)$ is consistent with the choice of a particular dynamical model in which the individual random microscopic events that contribute to the evolution of $P_n(t)$ occur independently, i.e., Poisson processes. In other words, we are assuming that no cooperative or coherent energy transfer processes occur within the system. For Poisson processes it is possible to devise a kinetic-based Monte Carlo method to solve the Master equation for which a clear relationship between Monte Carlo steps and real physical time can be established, thus making dynamical simulation using KMC possible.

KMC allows us to construct stochastic "trajectories" of the vibrational state of the entire system, $\{v_i(t)\}$, where v_i is the vibrational state of CO molecule i at time t. A two-dimensional square array of N adsorbed CO molecules with periodic boundary conditions was defined. The KMC algorithm proceeded as follows: (1) The initial vibrational state of each CO molecule in the system is chosen from a thermal Boltzmann distribution, noting, however, that at 22 K the probability of a CO molecule being vibrationally excited is negligible, and so the initial state of the system is $\{v_i(0)\} = 0$ for all $i = 1, ..., N$. (2) Given the current vibrational state of the system, $\{v_i(t)\}$, an inventory of all of the possible ways in which vibrational energy may flow into, out of, or within the CO monolayer is taken, and the rate constants for these possible microscopic events are summed (R is their sum). (3) One of the possible energy flow events is chosen to occur. This is done by arranging their rate constants as intervals on a line from 0 to R. A random number $u \cdot R$, where u is a uniformly distributed random number between 0 and 1, will correspond to one of the possible events. Events with large rates will occur more frequently than events with slow rates. (4) A time interval is obtained by evaluating $\Delta t = -\ln(u)/R$, where u is again a uniformly distributed random number between 0 and 1. This formula provides the appropriate distribution of time intervals between Poisson events that occur at a rate R.[21] (5) The vibrational trajectory is updated from $\{v_i(t)\}$ to $\{v_i(t+\Delta t)\}$. (6) Steps 2−5 are repeated to construct the entire dynamical trajectory. Once these trajectories are formed, the time-dependent average vibrational population distribution function, $P_n(t)$, can be computed by simply forming a histogram of the vibrational state of all the CO molecules in the system,

$\{v_i(t)\}$, at the appropriate time t and ensemble averaging over a sufficient number of trajectories.

III. Results

A. Isotope Effect. Chang and Ewing have extensively studied the CO/NaCl(100) system at 22 K using an isotopically pure sample of $^{13}C^{16}O$ and pumping the $n = 0 \rightarrow 1$ $^{13}C^{16}O$ vibrational transition with a 25 μJ pulse of 2107.4 cm^{-1} laser light with a temporal duration of 5 μs.[13] They then observed the subsequent fluorescence emanating from surface of the NaCl crystal as a function of time to learn about the vibrational dynamics of the CO monolayer. By using a series of optical filters to block fluorescence from reaching their detector, Chang and Ewing were able to infer the presence of CO molecules vibrationally excited in the range $2 \leq n \leq 15$. In a previous publication we used the vibrational energy flow rates and the KMC methods discussed in section II to simulate their experiment and obtain time-dependent vibrational population distributions, $P_n(t)$. The simulated time dependent vibrational population distributions show CO molecules excited over a similar range of quantum numbers observed in Chang and Ewing's experiment. We turn our attention now to the simulation of an experiment that has not been yet been performed, one in which the monolayer of CO molecules on the NaCl(100) surface contains more than just a single isotopomer of CO.

All of the simulations discussed in this paper were performed on a 16 × 16 square lattice with periodic boundary conditions. The lattice was found to be sufficiently large that simulations with larger lattices produced identical results for short-time test calculations of $P_n(t)$. Energy transfer rate constants were computed as discussed above, except that the rates of resonant energy transfer events were decreased by a factor of 1000. Even with this much slower rate, the singly excited CO molecules still make a sufficient number hops to be completely randomized before any other energy flow event takes place. This simplification leads to a tremendous computational benefit and was shown to converge to essentially the same results.

To illustrate the isotope effect on vibrational energy pooling in the CO/NaCl(100) we conducted simulations on a system containing 254 $^{12}C^{16}O$ molecules and 2 $^{13}C^{16}O$ molecules, approximately mirroring natural abundance. The pair of $^{13}C^{16}O$ molecules were placed as far apart from one another as is possible in the 16 × 16 square lattice of CO molecules that constitute our simulation box, remembering that periodic boundary conditions were employed. Energy enters the CO monolayer by exciting only those $^{12}C^{16}O$ molecules in their ground vibrational state, $n = 0$, to their first excited state, $n = 1$. For the first 5 μs of the simulation the rate constant for absorption of laser light, k_{abs}, was chosen to be 9×10^4 s^{-1} to match the absorption rate in Chang and Ewing's time dependent fluorescence experiment.[13] After the laser pulse duration of 5 μs passed, k_{abs} was set to zero eliminating further possibility of energy flowing into the CO monolayer.

The KMC algorithm provides a method for obtaining the time-dependent vibrational population distribution, $P_n(t)$, representing the probability of finding a CO molecule in vibrational state n at time t in the monolayer. Knowledge of $P_n(t)$ allows us to calculate the fluorescence intensity decay curve, $I(t)$, using the formula

$$I(t) = \frac{N}{A}\sum_{n=0}^{\infty} P_n(t)k_n \qquad (7)$$

where $N = 256$ is the number of molecules in the simulation cell, A is the area of the 16 × 16 lattice of CO molecules (4.01×10^{-13} cm^2), and k_n is the rate constant for single-photon fluorescence of a CO molecule from vibrational state n to $n - 1$, all of which can be obtained using standard spectroscopic relationships and the experimentally measured optical cross section for CO on the NaCl(100) surface ($\bar{\sigma}_z = 9.8 \times 10^{-18}$ cm molecule^{-1}).[17] $I(t)$ represents the flux of photons emanating from the surface at time t and has units photons·s^{-1}·cm^{-2}. The population distribution function, the fluorescence rate constants, and the number of molecules in the simulation cell are each different for the two isotopomers of CO, which allows us to calculate the fluorescence intensity decay appropriate for each. Shown in Figure 2 is the result for the fluorescence intensity decay, $I(t)$, for both $^{12}C^{16}O$ and $^{13}C^{16}O$ computed using eq 7. The time-dependent population distributions, $P_n(t)$, needed to compute $I(t)$ were constructed from 1000 independent vibrational state trajectories obtained using KMC methods, and the zero of time in the plot of $I(t)$ was taken from the end of the 5 μs pump pulse. Immediately apparent is that the flux of photons emanating from $^{13}C^{16}O$ molecules in the monolayer represents a sizable fraction of total fluorescence (10.7% at $t = 0$ ms and 23.2% at $t = 12$ ms) despite the fact $^{13}C^{16}O$ molecules comprised a mere 0.78% of the CO molecules in the simulation cell, 2 of 256. This observation suggests that $^{13}C^{16}O$ molecules preferentially receive more vibrational energy than do the much more abundant $^{12}C^{16}O$ molecules. The inset in Figure 2 focuses on the behavior of $I(t)$ during and shortly after the 5 μs period in which k_{abs} was nonzero, and thus $^{12}C^{16}O$ molecules could be excited from vibrational state $n = 0$ to $n = 1$. For $^{12}C^{16}O$ molecules, $I(t)$ grows nearly linearly for $t \leq 0$ as $^{12}C^{16}O$ molecules are directly excited by the laser. When the laser is turned off, the $I(t)$ curve for $^{12}C^{16}O$ undergoes an initial decay as energy rapidly pools and the total number of excited $^{12}C^{16}O$ molecules in the monolayer diminishes. For both $^{12}C^{16}O$ and $^{13}C^{16}O$ $I(t)$ decays on a millisecond time scale as energy is dissipated to the NaCl substrate. The initial growth in $I(t)$ for the heavy isotopomer $^{13}C^{16}O$ is qualitatively different because

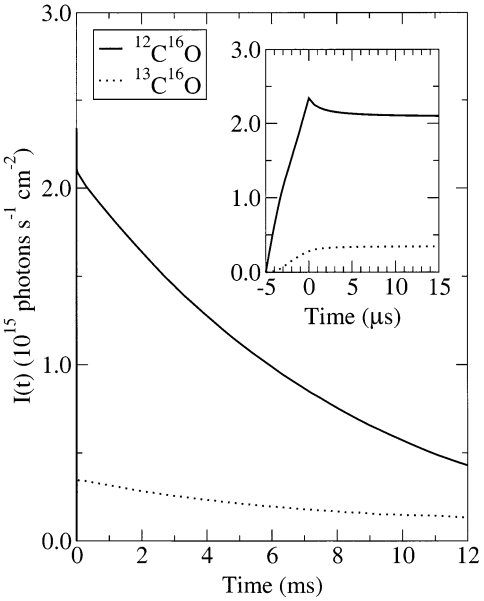

Figure 2. Simulation results for the integrated fluorescence intensity, $I(t)$, from $^{12}C^{16}O$ and $^{13}C^{16}O$ on NaCl(100) after being irradiated by a 25 μJ pulse for 5 μs, calculated using eq 7. The results shown are averages of 1000 independent 12 ms trajectories of the vibrational dynamics in a 16 × 16 square lattice of 254 $^{12}C^{16}O$ and 2 $^{13}C^{16}O$ molecules using periodic boundary conditions. The inset focuses on the short time behavior of $I(t)$.

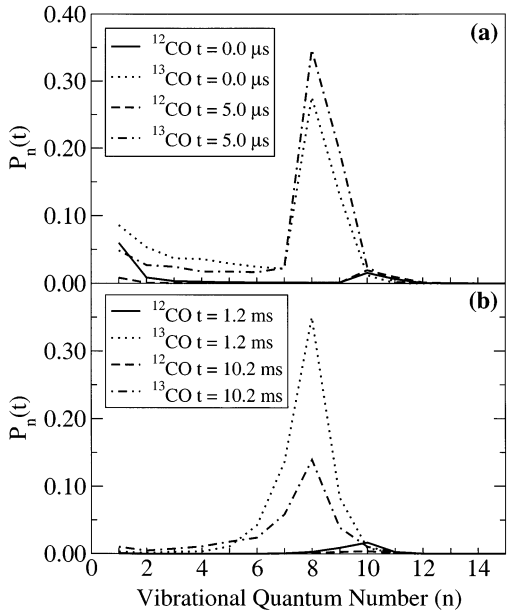

Figure 3. Simulated vibrational population distributions, $P_n(t)$, representing the average probability that a particular CO molecule on the NaCl(100) surface is in vibrational state n at time t after being irradiated by a 25 μJ pulse for 5 μs. The results shown are averages of 1000 independent trajectories of the vibrational dynamics in a 16 × 16 square lattice containing 254 $^{12}C^{16}O$ and 2 $^{13}C^{16}O$ molecules using periodic boundary conditions: (a) short-time vibrational population distributions; (b) long-time vibrational population distributions. All times are measured from the conclusion of the laser pulse.

$^{13}C^{16}O$ molecules are not directly excited by the laser but rather can only receive vibrational energy through nonresonant energy transfer events with neighboring vibrationally excited $^{12}C^{16}O$ molecules. Thus, the initial growth in $I(t)$ for $^{13}C^{16}O$ is quadratic, which is characteristic for a second-order excitation mechanism. Also, the fluorescence intensity does not reach a maximum as the laser is turned off at $t = 0$ for $^{13}C^{16}O$ as it does for $^{12}C^{16}O$. The maximum in $I(t)$ for $^{13}C^{16}O$ occurs at roughly 25 μs because it takes time for the energy to pool into the heavier isotope. Finally, note that $I(t)$ does not have an initial sharp decay for $^{13}C^{16}O$ as it does for $^{12}C^{16}O$. The fast initial decay for $^{12}C^{16}O$ is due to the rapid removal of laser excited $n = 1$ molecules via pooling. The $^{13}C^{16}O$ molecules are not excited by the laser.

More can be learned about the isotope effect in vibrational energy pooling in CO on NaCl(100) by considering the normalized time-dependent vibrational population distribution function, $P_n(t)$. In Figure 3a $P_n(t)$ is shown for both $^{12}C^{16}O$ and $^{13}C^{16}O$ at short times (0 and 5 μs) measured from the conclusion of the 5 μs excitation period in the simulation; longer times (1.2 and 10.2 ms) are shown in Figure 3b. The results shown represent averages of 1000 independent KMC trajectories, and the peaks corresponding to the probability of finding a CO molecule in its ground vibrational state, $P_0(t)$, have been omitted from each of the plots of $P_n(t)$ for clarity. Qualitatively, it is clear that for all times shown in Figure 3 a $^{13}C^{16}O$ molecule chosen at random in the system is much more likely to be found in an excited vibrational state than a $^{12}C^{16}O$ molecule. More quantitatively, the total probability of a CO molecule of a given isotopic composition being found in an excited vibrational state is given by

$$P_{ex}(t) = \sum_{n=1}^{\infty} P_n(t) = 1 - P_0(t) \qquad (8)$$

where the vibrational population distribution $P_n(t)$ is appropriate for the isotopomer under consideration. The total vibrational excitation probability, $P_{ex}(t)$, for both isotopes and each time slice in Figure 3 are listed in Table 2. At $t = 0.0$ μs it is already 9.0 times more likely for a $^{13}C^{16}O$ molecule in the sample to be vibrationally excited than for a $^{12}C^{16}O$ molecule. For short times after the 5 μs excitation period the probability that a given $^{12}C^{16}O$ molecule in the sample is excited decreases from 0.074 at $t = 0.0$ μs to 0.041 at $t = 5.0$ μs as vibrational energy is rapidly pooling decreasing the total number of vibrationally excited $^{12}C^{16}O$ molecules in the sample. By contrast, in the same time period, the probability that a given $^{13}C^{16}O$ molecule in the sample is excited increases from 0.666 to 0.721 as these heavier molecules continue to receive vibrational energy indirectly from neighboring $^{12}C^{16}O$ molecules. At longer times it becomes increasingly likely that a $^{13}C^{16}O$ molecule is excited relative to a $^{12}C^{16}O$ molecule, 19.5 times more likely at $t = 1.2$ ms and 31.9 times more likely at $t = 10.2$ ms.

TABLE 2: Total Probability, $P_{ex}(t)$, of Finding a CO Molecule in the KMC Simulation of CO on NaCl(100) of the Specified Isotope and at the Specified Time in *Any* Vibrationally Excited State ($n \geq 1$) Computed Using Eq 8[a]

time	$^{12}C^{16}O$	$^{13}C^{16}O$	time	$^{12}C^{16}O$	$^{13}C^{16}O$
0.0 μs	0.074	0.666	1.2 ms	0.033	0.642
5.0 μs	0.041	0.721	10.2 ms	0.010	0.319

[a] The simulation cell contains 254 $^{12}C^{16}O$ molecules and 2 $^{13}C^{16}O$ molecules, and the results shown represent the average of 1000 independent KMC trajectories. Times are measured relative to the conclusion of the 5 μs laser pulse.

Two important conclusions regarding the effect of isotopes on vibrational energy pooling in CO on NaCl(100) can be drawn by considering the results in Table 2 and Figures 2 and 3. (1) Vibrational energy preferentially pools on the heavier isotopomer, $^{13}C^{16}O$, and (2) vibrational energy persists for a longer time in $^{13}C^{16}O$. The observation that vibrational energy persists longer in $^{13}C^{16}O$ molecules seems to contradict the fact that for every value of the vibrational quantum number n the vibrational relaxation rate of $^{13}C^{16}O$ from vibrational state n to $n - 1$ exceeds that of $^{12}C^{16}O$. This apparent paradox can be resolved by noting that the most probable vibrational energy pool in a $^{12}C^{16}O$ molecule contains 10 vibrational quanta, and the most probable vibrational energy pool in a $^{13}C^{16}O$ molecule contains 8 vibrational quanta. This means that although vibrational energy preferentially pools on $^{13}C^{16}O$ molecules, on average these pools contain fewer quanta than pools on $^{12}C^{16}O$ molecules. Because the vibrational relaxation rate for a $^{12}C^{16}O$ molecule in vibrational state $n = 10$ exceeds the vibrational relaxation rate for a $^{13}C^{16}O$ in vibrational state $n = 8$, on average vibrational energy persists longer in $^{13}C^{16}O$ molecules than in $^{12}C^{16}O$ molecules.

Not coincidentally, the most probable number of vibrational quanta in a pool corresponds to the location of the first discontinuity in the fundamental vibrational energy pooling rate, $W_{1,n}$, as can be seen in Figure 1. For $^{12}C^{16}O$ the fastest vibrational energy pooling rate is $W_{1,9}$. The microscopic energy transfer event corresponding to this rate is $^{12}C^{16}O(1) + {}^{12}C^{16}O(9) \rightarrow {}^{12}C^{16}O(10) + {}^{12}C^{16}O(0)$, which forms $^{12}C^{16}O$ molecules with 10 vibrational quanta. Similarly, for $^{13}C^{16}O$ the fastest vibrational energy pooling rate is $W_{1,7}$, corresponding to $^{12}C^{16}O(1) + {}^{13}C^{16}O(7) \rightarrow {}^{12}C^{16}O(0) + {}^{13}C^{16}O(8)$, which forms $^{13}C^{16}O$ molecules with 8 vibrational quanta. For vibrational quantum numbers beyond the discontinuity in the fundamental vibrational energy pooling rate curve, vibrational relaxation can compete more effectively with vibrational exchange and begin attenuating vibrational energy pooling. At the modest excitation laser

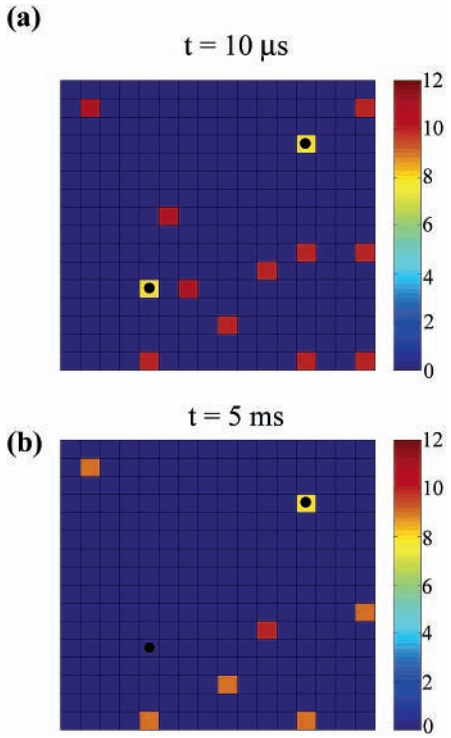

Figure 4. Two snapshots from a single KMC trajectory showing the vibrational states of the CO molecules in the 16 × 16 simulation cell containing 254 $^{12}C^{16}O$ and 2 $^{13}C^{16}O$ molecules at (a) $t = 10$ μs and (b) $t = 5$ ms, measured from the conclusion of the laser pulse. ● identifies the two $^{13}C^{16}O$ molecules.

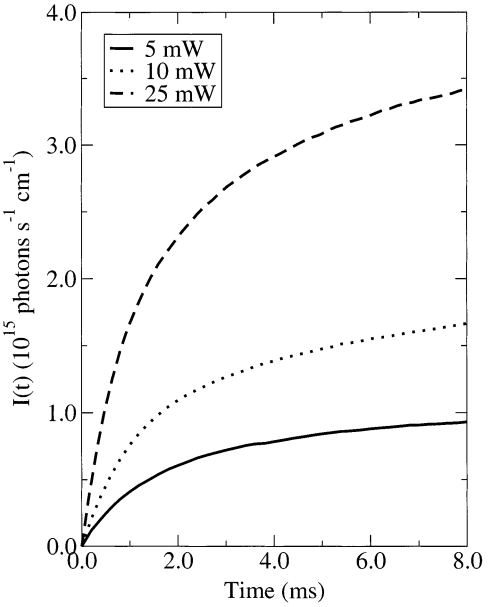

Figure 5. Simulation results of the steady-state integrated fluorescence intensity, $I(t)$, from a monolayer of pure $^{13}C^{16}O$ on NaCl(100) computed using eq 7 for three different CW laser intensities, 5 mW ($k_{abs} = 90$ s^{-1}), 10 mW ($k_{abs} = 180$ s^{-1}), and 25 mW ($k_{abs} = 450$ s^{-1}). The results shown are averages of 500 independent 12 ms trajectories of the vibrational dynamics in a 16 × 16 square lattice of $^{13}C^{16}O$ molecules using periodic boundary conditions.

intensity used in the current simulation, the number of vibrational quanta in the pools do not approach the ultimate limit, which occurs when vibrational relaxation rates exceed vibrational energy pooling rates ($n = 18$ for $^{12}C^{16}O$ and $n = 16$ for $^{13}C^{16}O$). The effect of excitation laser intensity on vibrational energy pooling in CO on NaCl(100) is explored more fully in section IIIB.

As time progresses, vibrational energy is lost to the underlying NaCl(100) substrate through vibrational relaxation processes. A manifestation of this energy loss is a decrease in the peak of the time dependent vibrational population distribution at $n = 8$ for $^{13}C^{16}O$ and $n = 10$ for $^{12}C^{16}O$ as time progresses. Note however as the system loses energy the peak in $P_n(t)$ does not move to lower values of the vibrational quantum number n as might be expected. Explaining why the peak remains stationary is explored in section IIIC, but its stationarity implies that CO molecules do not uniformly relax from high vibrational states to their ground vibrational state.

The KMC algorithm used to simulate the dynamics of vibrational energy flow in the CO/NaCl(100) system produces trajectories describing the vibrational state of each CO molecule in the simulation cell as a function of time, $\{v_i(t)\}$. A visual sense of the vibrational energy pooling phenomena can be obtained by considering snapshots of the vibrational state trajectory. Two snapshots chosen from a single KMC vibrational state trajectory are shown in Figure 4. The snapshot in Figure 4a shows the vibrational state of each CO molecule in the system 10 μs following the conclusion of the 5 μs excitation period. All 129 quanta of vibrational energy put into the system during the excitation period have pooled into just 11 $^{12}C^{16}O$ molecules and 2 $^{13}C^{16}O$ molecules. Note that both $^{13}C^{16}O$ molecules in the simulation cell are vibrationally excited and that the pools of vibrational energy on $^{13}C^{16}O$ molecules both contain 8 quanta compared to the pools on $^{12}C^{16}O$ molecules which contain either 10 or 11 quanta. The snapshot in Figure 4b was taken at $t = 5$ ms. By this time a significant amount of vibrational relaxation has occurred and 63 vibrational quanta remain in the system. The energy remaining in the system is pooled into 6 $^{12}C^{16}O$ molecules and one of the two $^{13}C^{16}O$ molecules.

B. Steady State. In this subsection we explore the effect of excitation laser intensity on vibrational energy pooling in CO on NaCl(100) by simulating a hypothetical experiment in which a continuous-wave (CW) laser is used to excite CO molecules from their ground vibrational state to their first excited vibrational state. Vibrational energy is continuously pumped into the system, but at the same time energy is being dissipated to the NaCl(100) substrate. After some time has passed these two processes balance one another and the vibrational state of the system will reach a steady state. This type of experiment, which has not yet been performed on the CO/NaCl(100) system, can be simulated using the KMC methods discussed in section IIB with the condition that the absorption rate, k_{abs}, is constant for the entire simulation, i.e., that it is not set to zero after some specified time to simulate a laser pulse. Different laser intensities simply correspond to different values for k_{abs}.

In Figure 5 we plot the fluorescence intensity curve, $I(t)$, for three different laser intensities, 5 mW ($k_{abs} = 90$ s^{-1}), 10 mW ($k_{abs} = 180$ s^{-1}), and 25 mW ($k_{abs} = 450$ s^{-1}). The simulation cell consisted of 256 $^{13}C^{16}O$ molecules arranged on a 16 × 16 square lattice, and the $I(t)$ curves were computed from 500 independent vibrational state trajectories using eq 7. In contrast to the laser pulse simulations the fluorescence intensity curves do not decay, but rather they grow as vibrational energy is put into the system and eventually level off to a constant as a signature of the system achieving a steady state. As expected, the time-dependent fluorescence intensity curves clearly demonstrate that more energy can be pumped into the system using lasers with higher intensities and that it is possible to achieve a steady state in the time scale of the KMC simulation.

More insight into the effect of laser intensity on the dynamics of vibrational energy flow in the CO/NaCl(100) system can be

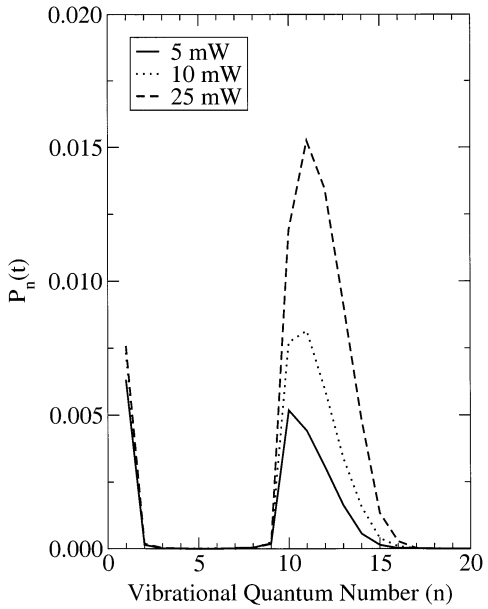

Figure 6. Simulated steady-state vibrational population distributions P_n, representing the average probability that a given CO molecule on the NaCl(100) surface is in vibrational state n at steady state. Three different laser intensities of $I = 5$ mW ($k_{abs} = 90$ s^{-1}), 10 mW ($k_{abs} = 180$ s^{-1}), and 25 mW ($k_{abs} = 450$ s^{-1}) were considered. The results shown are averages of 500 independent trajectories of the vibrational dynamics in a 16 × 16 square lattice of $^{13}C^{16}O$ molecules using periodic boundary conditions.

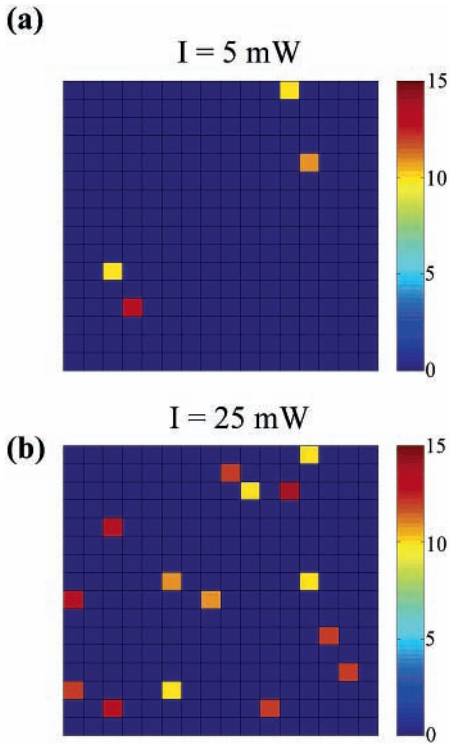

Figure 7. Snapshots from KMC trajectories of a monolayer of pure $^{13}C^{16}O$ on NaCl(100) showing the vibrational state of the $^{13}C^{16}O$ molecules in the 16 × 16 simulation cell at steady state under CW laser intensities of (a) $I = 5$ mW ($k_{abs} = 90$ s^{-1}) and (b) $I = 25$ mW ($k_{abs} = 450$ s^{-1}).

obtained by considering the steady-state vibrational population distributions shown in Figure 6. The large peak in the steady-state vibrational population distributions present in the range of vibrational quantum numbers from $n = 9$ to $n = 16$ is clear evidence for significant vibrational energy pooling. The magnitude of this peak grows with increasing excitation laser intensity confirming that more vibrational energy pools are present at steady state for higher laser intensities. In addition, the maximum in the peak is observed to move toward higher vibrational quantum numbers with increased excitation laser intensity. For $I = 5$ mW the maximum in the vibrational energy pooling peak of the steady state P_n curve occurs at $n = 10$, the same place it is found in all of the time-dependent vibrational population distributions for $^{13}C^{16}O$ shown in Figure 3. At higher laser intensities, $I = 10$ mW and $I = 25$ mW, the maximum in the vibrational energy pooling peak shifts to $n = 11$. Ultimately, the largest number of quanta that can pool on a single CO molecule is limited by vibrational relaxation. Examination of the rates of vibrational energy pooling and vibrational energy relaxation for $^{13}C^{16}O$ on NaCl(100) shows that, for vibrational energy states above $n = 16$, the rate of vibrational relaxation is faster than vibrational energy pooling. Therefore, a pool of 17 vibrational quanta on a $^{13}C^{16}O$ molecule on NaCl(100) cannot be sustained because the molecule can relax from $n = 17$ to $n = 16$ more quickly than it can be excited by an energy pooling process from $n = 16$ to $n = 17$. At low laser intensities there are simply too few quanta in the system to support vibrational energy pools approaching the $n = 16$ limit, but at higher laser intensities there are more vibrational energy pools present in the system, and the average number of vibrational quanta in these pools is increasing to approach the $n = 16$ limit. Note that, even at the highest laser intensity shown in Figure 5, $I = 25$ mW, there is essentially zero probability of finding $^{13}C^{16}O$ molecules in vibrational state $n = 17$ at steady state.

To get a sense of the extent of vibrational energy pooling in the steady-state simulations, it is useful to consider snapshots taken from the KMC vibrational-state trajectories. In Figure 7 snapshots depicting the vibrational state of each CO molecule in the simulation cell are shown at the end of two separate and randomly chosen 8 ms trajectories with two different excitation laser intensities, $I = 5$ mW and $I = 25$ mW. It is assumed that these two snapshots are representative examples of the vibrational state of the CO monolayer at steady state. It is immediately evident that there are more vibrational energy pools for the higher laser intensity (15) compared to the lower laser intensity (4). Furthermore, closer inspection of Figure 7 reveals that the average vibrational energy pool for the higher laser intensity contains more vibrational quanta (11.7) than the average vibrational energy pool for the lower laser intensity (11.0).

C. Finite vs Zero Temperature. In this subsection we return our consideration back to the time dependent fluorescence shown in Figure 3. Since the area under the $P_n(t)$ curve represents the total number of vibrational quanta in the system, the dissipation of vibrational energy to the bath is evidenced in Figure 3 by the decline in the peak at $n = 8$ for $^{13}C^{16}O$ and at $n = 10$ for $^{12}C^{16}O$. Although the overall area under the vibrational population distribution is expected to decline over time via vibrational relaxation, it is unexpected that the maximum in the vibrational population distribution should remain stationary. This implies that CO molecules are not uniformly relaxing back to their vibrational ground state through a process CO(n) → CO(n − 1) → ⋯ → CO(0), as this would cause the maximum in the vibrational population distribution to shift toward lower values of the vibrational quantum number n. Vibrational state snapshots of the CO monolayer, such as those shown in Figure 4, confirm that the total number of vibrational energy pools in the system decreases with time but that the number of quanta in the vibrational energy pools left in the system remains relatively constant as the system relaxes toward thermal equilibrium.

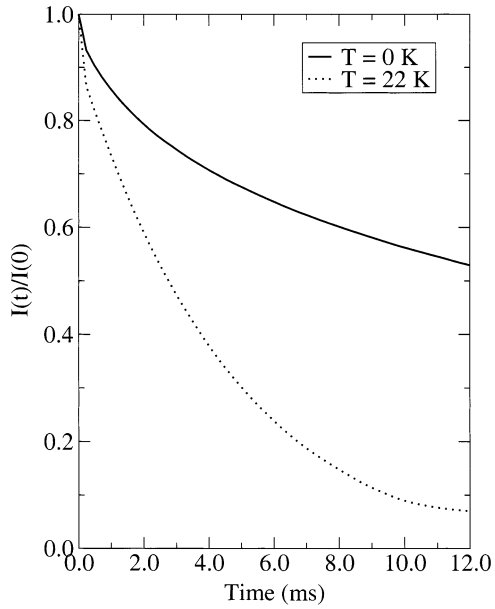

Figure 8. KMC simulation results for the integrated fluorescence intensity decay, $I(t)$, from a monolayer of pure $^{13}C^{16}O$ on NaCl(100) at $T = 0$ K and $T = 22$ K after being irradiated by a 25 μJ pulse for 5 μs, calculated using eq 7 and normalized by $I(0)$. The simulation results shown are averages of 1000 independent 12 ms trajectories of the vibrational dynamics in a 16 × 16 square lattice of $^{13}C^{16}O$ molecules using periodic boundary conditions.

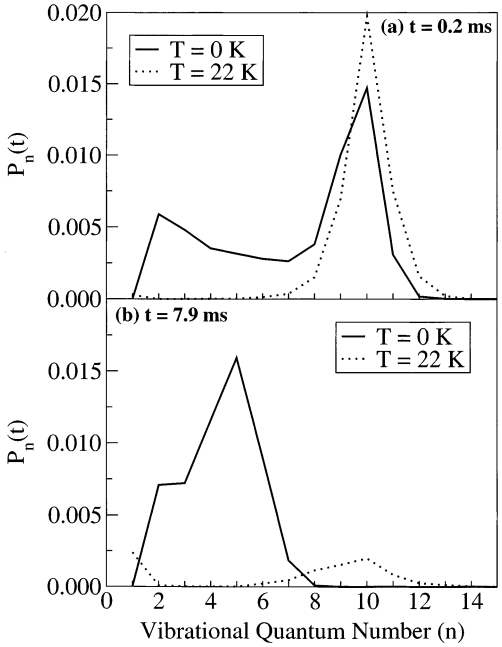

Figure 9. Shown are simulated vibrational population distributions, $P_n(t)$, representing the average probability that a given CO molecule on the NaCl(100) surface is in vibrational state n at time t after being irradiated by a 25 μJ pulse for 5 μs. The results shown are averages of 1000 independent trajectories of the vibrational dynamics in a 16 × 16 square lattice of $^{13}C^{16}O$ molecules using periodic boundary conditions: (a) short-time vibrational population distributions, $t = 0.2$ ms with (solid line) $T = 0$ K and (dotted line) $T = 22$ K; (b) long-time vibrational population distributions, $t = 7.9$ ms with (solid line) $T = 0$ K and (dotted line) $T = 22$ K. All times are measured from the conclusion of the 5 μs laser pulse.

Vibrational energy must be redistributing itself within the system, such that some pools disappear while others remain fully populated.

At zero temperature an energy transfer process of the type $CO(n) + CO(0) \rightarrow CO(n-1) + CO(1)$ is energetically uphill and cannot occur. The simulations that produced Figure 3 were carried out at 22 K, the temperature of the Chang and Ewing experiments. At 22 K it is still possible for some energetically uphill or "backward" vibrational energy hops to take place. The rate of backward vibrational energy hops increases for smaller values of the vibrational quantum number n, since less thermal activation energy is required for the energy hop to occur. In contrast, the rate of vibrational energy relaxation decreases for smaller values of the vibrational quantum number n. For a given temperature there is a critical point at which it is more likely for the vibrational energy pool to break apart, a single quantum at a time, via backward vibrational energy transfer with neighboring ground-state CO molecules, than for the molecule to undergo further vibrational relaxation. For $^{13}C^{16}O$ on NaCl-(100) at 22 K the rate of backward vibrational energy transfer exceeds the rate of vibrational relaxation for all vibrational quantum numbers $n \leq 9$. Thus, if a vibrational energy pool on a $^{13}C^{16}O$ molecule in a pure $^{13}C^{16}O$ monolayer on NaCl(100) relaxes to $n = 9$, it becomes more likely that it will redistribute its quanta to the other pools present in the system than to continue to uniformly relax toward its vibrational ground state. At finite temperature most of the energy that is dissipated from the CO monolayer into the NaCl substrate occurs from CO molecules vibrationally excited above $n = 9$. Redistribution of vibrational quanta allows the maximum in the vibrational population distribution to be maintained at $n = 10$ while the total number of vibrational energy pools decreases with time.

To further explore the effect of finite temperature we simulated the time dependent fluorescence experiment of Chang and Ewing as if it had been conducted at zero temperature. Assuming that the rate constants for forward vibrational energy hops and for vibrational relaxation are relatively insensitive to temperature in the range $0 \text{ K} \leq T \leq 22$ K, the time-dependent fluorescence experiment on a sample of pure $^{13}C^{16}O$ can be simulated at $T = 0$ K using $T = 22$ K rate constants for energetically downhill processes and simply not allowing any energetically uphill energy flow events to occur. In Figure 8 we show the simulated time-dependent fluorescence emanating from the $^{13}C^{16}O$/NaCl(100) system after it had been irradiated with a 5 μs pulse of laser light that delivers 25 μJ of energy at $T = 0$ K and $T = 22$ K. At $T = 22$ K the fluorescence intensity decays considerably more quickly than it does at $T = 0$ K. Furthermore, the fluorescence decay at finite temperature is nearly exponential, whereas at zero temperature the decay is highly nonexponential. Both observations are consistent with the argument that at zero temperature vibrational energy pools are completely stable and must decay uniformly to their vibrational ground state, but as the molecules begin to relax to lower vibrational states, the rate of vibrational relaxation becomes slower. Thus, it is completely expected that at zero temperature the overall fluorescence decay would be slower than the finite temperature fluorescence decay and that the zero temperature fluorescence decay would exhibit nonexponential behavior because the overall relaxation rate is changing with time. At finite temperature the general shape of the vibrational population distribution function remains stationary, and thus, there is a single overall vibrational relaxation rate that does not vary with time, which leads to the exponential fluorescence intensity decay observed in the experiment and in our simulations.

In Figure 9 we contrast the vibrational population distributions obtained for our simulation of the time-dependent fluorescence intensity experiment of Chang and Ewing at $T = 0$ K and $T = 22$ K. Figure 9a shows vibrational population distributions 0.2

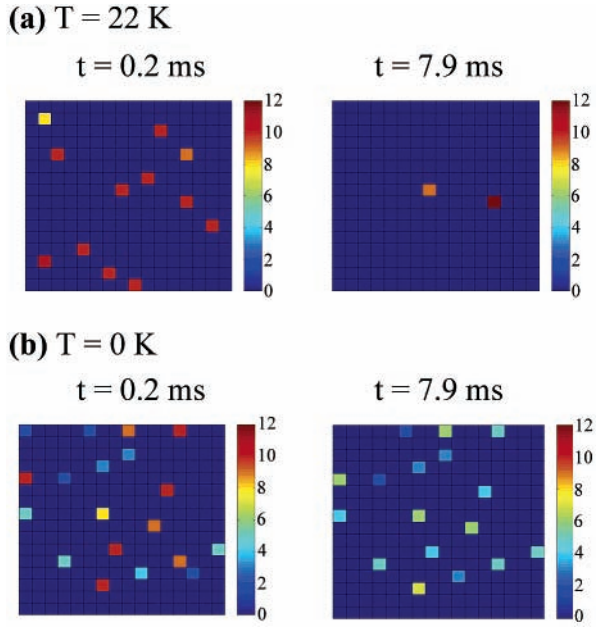

Figure 10. (a) Two snapshots from a single KMC trajectory showing the vibrational state of the $^{13}C^{16}O$ molecules in the 16 × 16 simulation cell at $T = 22$ K at $t = 0.2$ ms and $t = 7.9$ ms. (b) Two snapshots from a single KMC trajectory showing the vibrational state of the $^{13}C^{16}O$ molecules in the 16 × 16 simulation cell at $T = 0$ K at $t = 0.2$ ms and $t = 7.9$ ms.

ms from the conclusion of the 5 μs excitation period. Very little vibrational relaxation occurs on this relatively short time scale, but vibrational energy pooling is complete. Qualitatively, the finite temperature distribution function is sharply peaked and centered at $n = 10$, whereas the zero temperature distribution is broad spanning the range $2 \leq n \leq 12$. Once again, this demonstrates the increased stability of vibrational energy pools at zero temperature. At finite temperature a pool of $n = 2$ vibrational quanta is not stable in the presence of other larger pools; it will break apart into two single quanta that are free to migrate via resonant energy hops to enhance the size of the more stable larger pools. This process is analogous to Ostwald ripening of clusters.[48,49] In contrast, a pool of $n = 2$ quanta is completely stable at $T = 0$ K even in the presence of larger vibrational energy pools. The result is a much broader distribution of vibrational energy pools at 0 K than at 22 K. Figure 9b shows the vibrational population distributions at $t = 7.9$ ms. By this time a significant amount of vibrational energy relaxation has occurred. The peak at $n = 10$ in the finite temperature vibrational population distribution remains stationary from $t = 0.2$ ms to $t = 7.9$ ms, although the peak does become broader. Not surprisingly, the peak at $n = 10$ present in the zero temperature vibrational population distribution at $t = 0.2$ ms has shifted inward to $n = 5$ at $t = 7.9$ ms. This observation is consistent with the expected *uniform* relaxation of highly vibrationally excited CO molecules toward their ground state at zero temperature.

Finally, vibrational state snapshots from the KMC simulations of the time dependent fluorescence intensity experiment are shown in Figure 10 for $T = 22$ K and $T = 0$ K. For each temperature, snapshots at $t = 0.2$ ms and $t = 7.9$ ms are taken from the same randomly chosen vibrational state trajectory. At $t = 0.2$ ms there is roughly the same total number of vibrational quanta present in both the finite and zero temperature snapshots; however, the quanta are distributed to more vibrational energy pools in the zero temperature snapshot (19) compared to the finite temperature snapshot (12). By $t = 7.9$ ms most of the vibrational quanta in the $T = 22$ K simulation have dissipated leaving just two pools with roughly the same number of quanta in each as the pools at $t = 0.2$ ms. The $t = 7.9$ ms snapshot of the vibrational state of the $T = 0$ K system is very different in that 17 of the original 19 vibrational energy pools remain, albeit with less vibrational quanta in each.

IV. Concluding Remarks

In this paper we have explored the vibrational dynamics in the CO/NaCl(100) system using kinetic Monte Carlo simulations with theoretical rate constants for various channels of vibrational energy flow as input. We predict a dramatic isotope effect in which energy preferentially pools on heavier isotopomers of CO if a natural abundance sample of CO is optically pumped. Using simple optical pumping to preferentially pool energy onto heavy diatomic isotopomers on a surface could cause these species to be more chemically reactive than their lighter counterparts and form the basis of a method for performing isotopically selective chemistry. Our simulations of the steady-state vibrational population distributions for a CO/NaCl(100) system pumped by a continuous laser source demonstrate that vibrational energy pools containing more and more quanta can be formed by pumping with more intense lasers until a theoretical crossover is reached where vibrational relaxation rates become faster than vibrational energy pooling rates. This crossover occurs at $n = 18$ for $^{12}C^{16}O$. Finally, the effect of temperature on the vibrational dynamics in the CO/NaCl(100) system was explored with the result that finite temperature allows for energy redistribution within the monolayer, hastening vibrational relaxation.

Acknowledgment. The authors thank Professor George Ewing for helpful discussion of this work and the National Science Foundation for support through Grant CHE-0075744. S.A.C. also acknowledges the support of a National Science Foundation Graduate Research Fellowship.

References and Notes

(1) Ewing, G. E. *Int. Rev. Phys. Chem.* **1991**, *10*, 391.
(2) Ewing, G. E. *Acc. Chem. Res.* **1992**, *25*, 292.
(3) Heidberg, J.; Stahmer, K. W.; Stein, H.; Weiss, H. *J. Electron Spectrosc. Relat. Phenom.* **1987**, *45*, 87.
(4) Richardson, H. H.; Ewing, G. E. *J. Chem. Phys.* **1987**, *91*, 5883.
(5) Chang, H.-C.; Richardson, H. H.; Ewing, G. E. *J. Chem. Phys.* **1988**, *89*, 7561.
(6) Richardson, H. H.; Chang, H.-C.; Noda, C.; Ewing, G. E. *Surf. Sci.* **1989**, *216*, 93.
(7) Noda, C.; Ewing, G. E. *Surf. Sci.* **1990**, *240*, 181.
(8) Disselkamp, R.; Chang, H.-C.; Ewing, G. E. *Surf. Sci.* **1990**, *240*, 193.
(9) Schmicker, D.; Toennies, P.; Vollmer, R.; Weiss, H. *J. Chem. Phys.* **1991**, *95*, 9412.
(10) Gready, J. E.; Bacskay, G. B.; Hush, N. S. *Chem. Phys.* **1978**, *31*, 375.
(11) Merideth, A. W.; Stone, A. J. *J. Chem. Phys.* **1996**, *104*, 3058.
(12) Hoang, P. N. M.; Picaud, S.; Girardet, C.; Merideth, A. W. *J. Chem. Phys.* **1996**, *105*, 8453.
(13) Chang, H.-C.; Ewing, G. E. *Phys. Rev. Lett.* **1990**, *65*, 2125.
(14) Chang, H.-C.; Ewing, G. E. *J. Phys. Chem.* **1990**, *94*, 7635.
(15) Chang, H.-C.; Ewing, G. E. *J. Electron Spectrosc. Relat. Phenom.* **1990**, *54/55*, 39.
(16) Noda, C.; Richardson, H. H.; Ewing, G. E. *J. Chem. Phys.* **1990**, *92*, 2099.
(17) Chang, H.-C.; Ewing, G. E. *Chem. Phys.* **1989**, *139*, 55.
(18) Treanor, C. E.; Rich, J. W.; Rehm, R. G. *J. Chem. Phys.* **1968**, *48*, 1798.
(19) Ashcroft, N. W.; Mermin, N. D. *Solid State Physics*; Holt, Rinehart and Winston: New York, 1976.
(20) Corcelli, S. A.; Tully, J. C. *J. Chem. Phys.* **2002**, *116*, 8079.
(21) Fichthorn, K.; Weinberg, W. H. *J. Chem. Phys.* **1991**, *95*, 1090.
(22) Lu, Y.-T.; Metiu, H. *Surf. Sci.* **1991**, *245*, 150.

(23) Maksaym, P. A. *Semicond. Sci. Technol.* **1988**, *3*, 594.
(24) Metiu, H.; Lu, Y.-T.; Zhang, Z. *Science* **1992**, *255*, 1088.
(25) Voter, A. F. *Phys. Rev. B* **1986**, *34*, 6819.
(26) Lee, W.; Adamovich, I. V.; Lempert, W. R. *J. Chem. Phys.* **2001**, *114*, 1178.
(27) Corcelli, S. A. Ph.D. Thesis, Yale University, 2002.
(28) Hsu, D.; Skinner, J. L. *J. Chem. Phys.* **1984**, *81*, 5471.
(29) DiBartolo, B. *Optical Interactions in Solids*; Wiley: New York, 1968.
(30) Egorov, S. A.; Skinner, J. L. *J. Chem. Phys.* **1995**, *103*, 1533.
(31) Trenary, M.; Uram, K. H.; Bozso, F.; Yates, J. T., Jr. *Surf. Sci.* **1984**, *146*, 269.
(32) Persson, B. N. J.; Ryberg, R. *Phys. Rev. B* **1981**, *24*, 6954.
(33) Lucchese, R. R.; Tully, J. C. *J. Chem. Phys.* **1984**, *80*, 3451.
(34) Legay-Sommaire, N.; Legay, F. *IEEE J. Quantum Electron.* **1980**, *QE-16*, 308.
(35) Turnidge, M. L.; Reid, J. P.; Barnes, P. W.; Simpson, C. J. S. M. *J. Chem. Phys.* **1998**, *108*, 485.
(36) Coletti, C.; Billing, G. D. *J. Chem. Phys.* **1999**, *111*, 3891.
(37) Hsu, D.; Skinner, J. L. *J. Chem. Phys.* **1984**, *81*, 5471.
(38) Persson, B. N. J. *J. Phys. C: Solid State Phys.* **1984**, *17*, 4741.
(39) Persson, B. N. J.; Ryberg, R. *Phys. Rev. B* **1989**, *40*, 10273.
(40) Benjamin, I.; Reinhardt, W. P. *J. Chem. Phys.* **1989**, *90*, 7535.
(41) Partlow, W. D.; Moos, H. W. *Phys. Rev.* **1967**, *157*, 252.
(42) Weber, M. J. *Phys. Rev. B* **1973**, *8*, 54.
(43) Miller, M. P.; Wright, J. C. *J. Chem. Phys.* **1979**, *71*, 324.
(44) Zhang, G.; Ying, X.; Yao, L.; Chen, T.; Chen, H. *J. Lumin.* **1994**, *59*, 315.
(45) Heilweil, E. J.; Casassa, M. P.; Cavanagh, R. R.; Stephenson, J. C. *Chem. Phys. Lett.* **1985**, *117*, 185.
(46) Casassa, M. P.; Heilweil, E. J.; Stephenson, J. C.; Cavanagh, R. R. *J. Chem. Phys.* **1986**, *84*, 2361.
(47) Happek, U.; Mungan, C. E.; von der Osten, W.; Sievers, A. J. *Phys. Rev. Lett.* **1994**, *72*, 3903.
(48) Chakraverty, B. K. *J. Phys. Chem. Solids* **1967**, *28*, 2401.
(49) Lifshitz, I. M.; Slyozov, V. V. *J. Phys. Chem. Solids* **1961**, *19*, 35.